Nanomedicine: Nanotechnology, Biology, and Medicine
21 (2019) 102035

nanomedjournal.com

Structural and positional impact on DNAzyme-based electrochemical sensors for metal ions

Xudong Guo, MS[a,b,1], Min Li, PhD[c,1], Rongtao Zhao, PhD[b], Yi Yang, MS[b], Ruili Wang, PhD[b], Feng Wu, MS[b], Leili Jia, PhD[b], Yuxi Zhang, BS[b], Lihua Wang, PhD[d], Zhibei Qu, PhD[e,f], Fei Wang, PhD[e,f], Ying Zhu, PhD[d], Rongzhang Hao, PhD[a,b,*], Xueli Zhang, PhD[e,f,**], Hongbin Song, MD[a,b,*]

[a]*Academy of Military Medical Sciences, Academy of Military Sciences, Beijing, China*
[b]*Chinese PLA Center for Disease Control and Prevention, Beijing, China*
[c]*Institute of Molecular Medicine, Renji Hospital, Shanghai Jiao Tong University School of Medicine, Shanghai, China*
[d]*Division of Physical Biology & Bioimaging Center, Shanghai Institute of Applied Physics, Chinese Academy of Science, Shanghai, China*
[e]*Joint Research Center for Precision Medicine, Shanghai Jiao Tong University & Affiliated Sixth People's Hospital South Campus, Shanghai, China*
[f]*Southern Medical University Affiliated Fengxian Hospital, Shanghai, China*

Revised 24 May 2019

Abstract

The rapid, accurate and convenient detection of heavy metal is very important to public health. Here, we developed a DNAzyme-based electrochemical sensor for Pb^{2+}. A DNAzyme-including and Pb^{2+} active probe was anchored to the biosensing interface, based on the well-defined self-assembled, three-dimensional DNA nanostructure. The results indicate that the detection performance depends on the change of distances between the methylene blue and the electrode surface. The limit of detection (LOD) could reach the concentration of 0.01 μM Pb^{2+}, and the signal change shows semi-logarithmic relationship with the concentration of Pb^{2+} from 0.01 μM to 100 μM. The biosensor also presents good stability and specificity to detect Pb^{2+} in tap or river water. This method not only provides promising approach for improving the performance of tetrahedra in detecting Pb^{2+}, but helps deepen the understanding of tetrahedral structure design and how the position of electroactive groups affects the performance of electrochemical sensing.

Key words: DNAzyme; Heavy metal ion; DNA tetrahedron; Electrochemical biosensor; Methylene blue

Lead ion (Pb^{2+}) is an important pollutant that can cause serious physical damage, including abdominal pain, irritability, headaches, memory problems, and constipation.[1,2] Current methods for detecting Pb^{2+} require inductively coupled plasma/mass spectroscopy (ICP/MS),[3] a rather complex laboratory technique. The selective electrode is also a widely used method for detecting lead ion, despite of its high limit of detection (LOD) and less sensitivity.[4] Many efforts have been made for quick, easy, and sensitive detection of lead ions.[5–10] The catalytic activity of DNAzymes is metal ion cofactor-dependent, as in the case with some proteins.[11–15] Much research has focused on the 8-17 DNAzyme owing its high specificity for Pb^{2+}.[16–19] The 8-17 DNAzyme has a specific sequence, and its complementary substrate chain contains only one RNA adenine. In the presence of lead ions, the 8-17 DNAzyme cuts and sheds the substrate chain.[20–22]

Xiao et al riveted the 8-17 DNAzyme sequence to a gold electrode interface using a covalent modification method and, in the presence of Pb^{2+}, the trans-acting catalytic strand cleaved the

Disclosure: This work was funded by the Mega-projects of Science and Technology Research (grant numbers 2018ZX10711001 and 2017ZX10304403), the National Natural Science Foundation of China (grant number 81871738), and the National Key R&D Program of China (grant number 2017YFC1200403).

*Corresponding authors at: Academy of Military Medical Sciences, Academy of Military Sciences, Beijing, China.

**Correspondence to: X Zhang, Joint Research Center for Precision Medicine, Shanghai Jiao Tong University & Affiliated Sixth People's Hospital South Campus, Shanghai, China.

E-mail addresses: hrongzhang@163.com (R. Hao), lejing1996@aliyun.com (X. Zhang), hongbinsong@263.net (H. Song).

[1] These authors contributed equally to the work.

https://doi.org/10.1016/j.nano.2019.102035
1549-9634/

sessile phosphodiester of the substrate into two pieces at the ribonucleotide site. By electrochemically measuring the change in the current value, a detection limit of 0.3 μM was achieved.[23] However, the detection performance can be markedly affected by the single-strand surface probe jamming effect, probe intertwining, lodging, and non-specific adsorption. Yun et al used a colorimetric method to detect lead ions using a DNAzyme to cleave the substrate, and the sheared product was combined with nanogold to detect lead ions with a detection limit of 5 nM.[24] However, the colorimetric method involves visual observation (which is not accurate) and requires a large optical instrument. Currently, with the development of nanotechnology, a variety of approaches based on nanomaterials have been used in the sensing field,[25–31] such as DNA tetrahedron which is a nanostructure formed by equal mixing and annealing of four single-stranded DNAs.[32–38] Because DNA obeys specific A-T and G-C base pairing rules, it is possible to precisely control the size of tetrahedral DNA nanostructures and introduce functionalized sequences. The three-dimensional (3D) DNA tetrahedron applied in electrochemical biosensors offers a great advantage in the field of sensing.[8,39–42]The three vertices of the tetrahedron probe are modified with a thiol group and fixed to the surface of the gold electrode. The distance between the probes can be controlled to ensure the desired orientation. The tetrahedral structure has a certain thickness (~6 nm) and provides a solution-like environment. The reaction environment improves the affinity and enables good target detection.[40–48] Zhou et al embedded a DNAzyme into one side of a DNA tetrahedron and detected Pb^{2+} by fluorescence with a detection limit of 3.9 nM in cells.[49] However, detecting lead ions by fluorescence is cumbersome and reading the fluorescent signals requires a large instrument.

To solve these problems and explore the impact of the DNA tetrahedral structure and methylene blue electrochemical active position on the DNAzyme-based signal response to Pb^{2+}, we combined DNA tetrahedral electrochemical biosensing technology and DNAzyme-based targeted RNA-cleavage technology to establish a lead-ion detection platform. Initially, we designed a detection model (Model A) by referring to Xiao's[23] electrochemical scheme and replaced one edge of the tetrahedron with a DNAzyme. Contrary to our expectation, the detection signal decreased instead of increased upon Pb^{2+} binding, which was due to steric hindrance on the surface of the gold electrode. Thus, we designed Model B and Model C to achieve lower detection limit of lead ions. Based on these detection models, we explored the influence of the distance between the electroactive groups and the gold electrode surface on the detection performance.

Methods

Chemicals and materials

Tris(2-carboxyethyl)-phosphine hydrochloride (TCEP) and 6-mercaptohexanol (MCH) were purchased from Sigma-Aldrich. $Pb(OAc)_2{\cdot}3H_2O$, $Zn(OAc)_2{\cdot}2H_2O$, $Co(OAc)_2{\cdot}4H_2O$, $Mn(OAc)_2{\cdot}4H_2O$, $Ni(OAc)_2{\cdot}4H_2O$, $Ca(OAc)_2{\cdot}H_2O$, and $Mg(OAc)_2{\cdot}4H_2O$ were purchased from Sigma-Aldrich and used without further processing. All metal acetate was dissolved in 10% CH_3COOH as a 0.1 M stock solution. Further dilution was performed with 50 mM acetic acid. The following buffers were used in the experiments: TM buffer (50 mM Tris-acetate, 1 M NaCl, pH 6.5; used to form DNA tetrahedra) and soaking buffer (50 mM Tris, 0.5 M NaCl, pH 6.5). DNA oligonucleotides with the following sequences (from 5′ to 3′) were synthesized and purified by Takara Biotechnology, Inc. (Shanghai, China):

Strand AZM: MB-TTCATCTCTTCTCCGAGCCGGTCG AAATAGTGAGTACATTACAGCTTGCTACACGAG AAGAGCCGCCATAGTA.

Strand AZ: TTCATCTCTTCTCCGAGCCGGTCGAA ATAGTGAGTACATTACAGCTTGCTACACGA GAAGAGCCGCCATAGTA.

Strand B: SH-TATCACCAGGCAGTTGACAGTG TAGCAAGCTGTAATAGATGCGAGGGTCCAATAC.

Strand C: SH-TCAACTGCCTGGTGATAAAACG ACACTACGTGGGAATCTACTATGGCGGCTCTTC.

Strand D: GCTTCCCACGTAGTGTCGTTTGTATTGGA CCCTCGCAT-SH.

Strand DS: ACTCACTATrAGGAAGAGATGGCTT CCCACGTAGTGTCGTTTGTATTGGACCCTCGCAT-SH.

Strand DSM: MB-TTACTCACTATrAGGA AGAGATGGCTTCCCACGTAGTGTCGTTTGTA TTGGACCCTCGCAT-SH.

Strand substrate: ACTCACTATrAGGAAGAGATG.

Detection Model A involved the use of five strands: AZM, B, C, D, and the strand substrate. Detection Model B involved four strands: AZM, B, C, and DS. Detection Model C also involved four strands: AZ, B, C, and DSM. M refers to a chain with the modifications of electrochemically active group (methylene blue, MB), and rA refers to an adenine ribonucleotide).

Instruments

Electrochemical measurements were performed on a CHI 760E electrochemical workstation (CH Instruments Co., Shanghai, China). A conventional three-electrode system including a gold electrode (2 mm in diameter) as the working electrode, an Ag/AgCl electrode (3 M KCl) as the reference electrode, and a platinum wire as the auxiliary electrode was used for cyclic voltammetry (CV) and square wave voltammetry (SWV). CV was carried out from 0 to 0.7 V at a scan rate of 100 mV/s. SWV was carried out from 0.5 to 0 V at a frequency of 50 Hz with an amplitude of 50 mV.

Methods

In the beginning, we designed Model A, which is an incomplete tetrahedron formed by the annealing of five strands including strand AZM, strand B, strand C, strand D, and the substrate strand. The 5′ end of the A chain was modified with MB, and the substrate strands were later hybridized with it. The edge of the tetrahedron containing DNAzyme was free to move in solution. After the addition of lead ions, the phosphodiester bond at the rA of the substrate chain was cleaved into two pieces. Since the free energy was reduced, both pieces of the substrate were latterly shed from the tetrahedron, and the A chain was opened from the neck ring structure to a single-stranded state. Then, the distance between the MB to the electrode surface

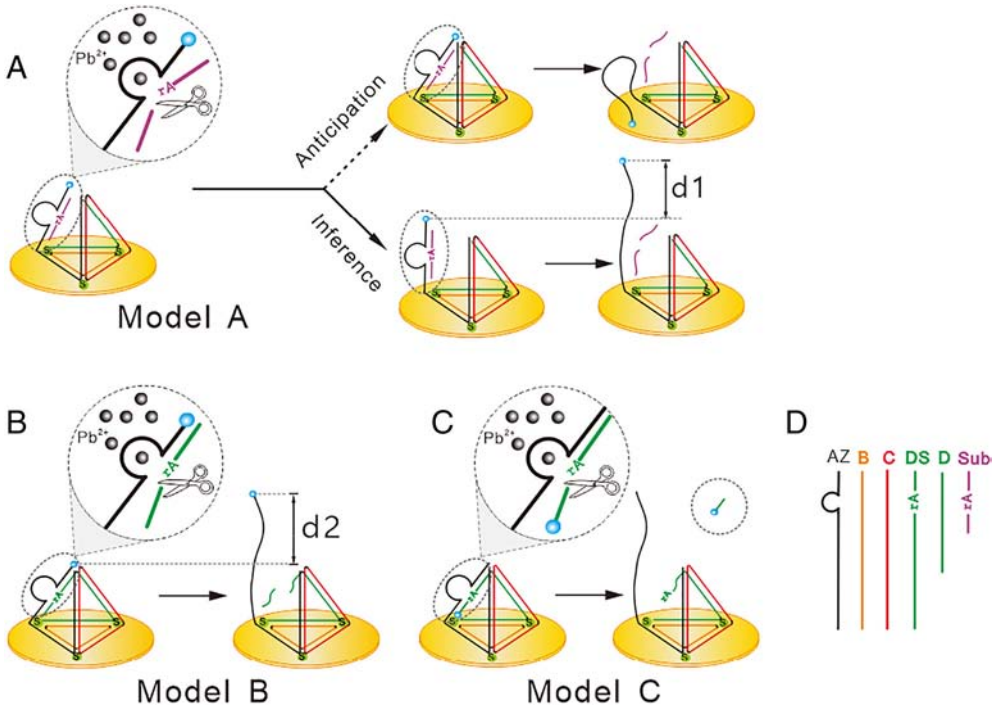

Figure 1. Schematic illustration of tetrahedral DNAzyme-based enzymatic cleavage. **(A)** Two hypothetical types of structural changes occurring in the presence of lead ions in Model A. **(B)** Structural change occurring in the presence of lead ions in Model B. **(C)** Structural change occurring in the presence of lead ions in Model C. **(D)** DNA strands making up the DNA tetrahedron.

increased. In anticipation, we initially considered that the chain modified with MB would be free in solution and have a certain degree of flexibility. The electroactive group collides freely with the surface of the electrode, and an increased electrochemical signal could be displayed as also described by Xiao Yi in his single-stranded electrochemical detection procedure. Interestingly, the signal decreased after adding lead ions. This phenomenon may be due to steric hindrance of the tetrahedron, as shown by inference in Figure 1, *A*. To investigate the effect of the position of modification of the electroactive group and the tetrahedron structure on the detection performance, we designed Model B (Figure 1, *B*) and Model C (Figure 1, *C*). Model B involves a complete tetrahedron formed by the annealing of strands AZM, B, C, and DS. The substrate chain is integrated into the tetrahedral strand D as DS. MB is also modified at the 5′ end of the A chain. In the presence of lead ions, the DNAzyme cleaves the substrate. Thus, the A chain is free in solution and the distance of the MB label from the electrode surface is increased. Model C involves a complete tetrahedron formed by the annealing of strands AZ, B, C, and DSM, where the 5′ end of the D chain is modified with MB (Figure 1, *C*). In the presence of lead ions, the DNAzyme cleaves the substrate strand into two pieces at the ribonucleotide site, and the substrate chain with the MB is detached from the tetrahedron. We assembled the synthesized tetrahedron onto the surface of the gold electrode and recorded the absolute current values of the three models every two minutes using SWV. Wait until the current value stabilizes (as shown in Figure S1 in the Supporting Information) to calculate the percentage change in current value before and after the reaction.

Synthesis and characterization of DNA tetrahedra

For each model (Model A: strands AZM, B, C, D, and the substrate strand; Model B: strands AZM, B, C, and DS; Model C: strands AZ, B, C, and DSM), the strands were dissolved in TM buffer, and the mixtures were heated at 95 °C for 10 min and quickly cooled down to 4 °C within 1 min, yielding a final DNA tetrahedra concentration of 1 μM. Each set of tetrahedral constituent chains is mixed and annealed to form a tetrahedral nanostructure, and then verified by polypropylene gel electrophoresis. The details of the polyacrylamide gel electrophoresis method are given in Table S1 in the Supporting information.

Preparation of self-assembling DNA tetrahedra on gold electrodes

Before preparing self-assembling DNA tetrahedra, gold electrodes were first electrochemically cleaned in 0.5 M NaOH. Then, the gold electrodes were polished for 2 min using a microcloth with 0.3 and 0.05 μm γ-alumina particles. Then, the polished electrodes were sonicated in ethanol and Milli-Q water (3 min for each sonication step). Next, the electrodes were electrochemically cleaned in 0.5 M H_2SO_4 by scanning the potential between the oxidation and reduction of gold (0.35 and 1.5 V, respectively), and finally the electrodes were cycled in 0.5 M H_2SO_4/0.01 M KCl. To determine the

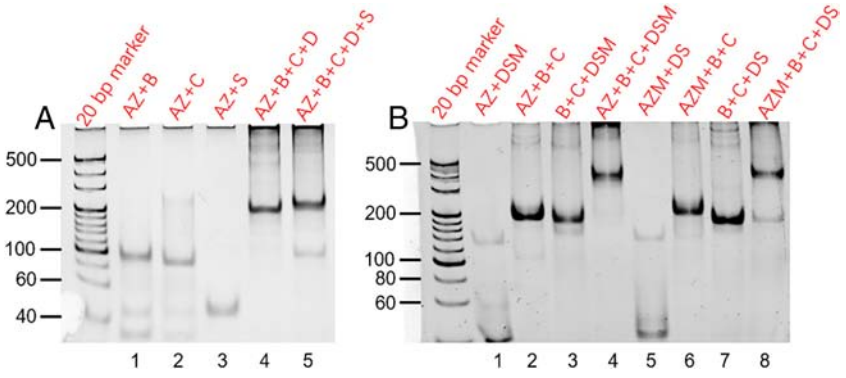

Figure 2. PAGE (8%) analysis of the self-assembled DNA strands using all possible combinations of the four strands. The bands in panel **A** (lanes 1-3) and panel **B** (lanes 1-3, 5-7) feature a common tailing phenomenon, suggesting that the hybridization between two or three strands was incomplete. The concentration of all strands was 1 μM. **(A)** Lane 4 represents AZM, B, C, D, four chains consisting of non-intact tetrahedra. Lane 5 represents AZM, B, C, D, substrate, five chains form non-integral tetrahedra. **(B)** Lane 4 and lane 8 show complete tetrahedral PAGE bands for the Model B and Model C designs, respectively.

effective active surface area, the electrodes were scanned in 0.05 M H_2SO_4. After cleaning the electrodes, 3 μL of 1 μM DNA tetrahedron, which was annealed in TM buffer with 3 mM TCEP, was incubated overnight on the freshly cleaned gold electrodes at room temperature to form a self-assembled monolayer.

Procedures for electrochemical measurement

DNA tetrahedra were used to form a self-assembled monolayer on the electrode. Then, the modified electrodes were exposed to a 2 mM MCH solution in phosphate-buffered saline (pH 6.5; 50 mM Tris, 1 M NaCl) at room temperature for 1 h to avoid interference from oxygen, which shows a similar reduction potential to that of MB. After the blockage, the electrodes were transferred to soaking buffer for 1 h. Next, the current signal response was interrogated by CV and SWV. For enzymatic cleavage reactions, the electrode was reacted with various concentrations of target Pb^{2+} in buffered Tris (50 mM Tris-acetate 0.5 M NaCl, pH 6.5) for 60 min at room temperature to achieve maximum substrate cleavage on the gold surface, after which the electrodes were transferred (within 1 h) to buffered Tris (pH 6.5) and thoroughly washed to remove the substrate chain. Control electrodes were prepared in an identical fashion.

Results

Characteristic of DNA tetrahedra

The assembly of the DNA tetrahedra was characterized by polyacrylamide gel electrophoresis (PAGE), and cross-hybridizations between two or three strands during the thermal annealing process were also evaluated. Inspection of Figure 2 reveals that the bands in Figure 2, *A* (lanes 1-3) and Figure 2, *B* (lanes 1-3, 5-7) featured a common tailing phenomenon, suggesting that incomplete hybridization occurred between the two or three strands. In contrast, when all strands were combined in equimolar quantities, a clearly independent and non-trailing band with much lower electrophoretic mobility was observed (lanes 4 and 5 in Figure 2, *A*, lanes 4 and 8 in Figure 2, *B*).

Characterization of the enzyme cleavage reaction

To analyze the enzymatic cleavage reaction, we used PAGE to characterize the DNAzyme-based tetrahedron cleavage products. Figure 3, *A* and *B* shows enzymatic cleavage results in polyacrylamide gels with concentrations of 8% and 15%, respectively, using Model A. The results obtained with the 8% polyacrylamide gel showed that the bands for tetrahedra that hybridized to the substrate chains (Figure 3, *A*, AZ + B + C + D) had a lower electrophoretic mobility than those that did not hybridize to the substrate chains (Figure 3, *A*, AZ + B + C + D + S). After the addition of lead ions, the tetrahedron band (Figure 3, *A*, AZ + B + C + D + Pb^{2+}) showed a higher electrophoretic mobility than the tetrahedron band that hybridized to the substrate chain (Figure 3, *A*, AZ + B + C + D + S). The migration distance of the band (Figure 3, *A*, AZ + B + C + D + Pb^{2+}) was the same as the tetrahedral bands that did not hybridize with the substrate (Figure 3, *A*, AZ + B + C + D). This phenomenon indicates that the substrate strand was capable of hybridizing to the enzyme strand and then could be successfully cleaved in the presence of lead ions. After the addition of lead ions, a new band appeared as shown by the black arrow in Figure 3. This new band was the substrate-cleavage product, and the band provides strong evidence that the enzymatic cleavage reaction occurred.

Figure 3, *C* and *D* shows the polyacrylamide gels for Model B and Model C at concentrations of 8% and 15%, respectively. The 8% polyacrylamide gel shows that, after the addition of lead ions, the bands for the tetrahedra showed a higher electrophoretic mobility (versus the absence of Pb^{2+}), which indicates that a cleavage reaction occurred in the presence of Pb^{2+} and that the substrate chain detached from the tetrahedron after cleavage. The 15% polyacrylamide gel shows that, after adding lead ions, a new band was formed, i.e., the substrate-cleavage product (shown by the arrow). These two phenomena indicate that the enzymatic cleavage reaction occurred.

Electrochemical signal responses of three detection models

As shown in Figure 4, *A*, the DNAzyme-based tetrahedron sensor has a very strong response to the presence of Pb^{2+}.In the absence of Pb^{2+}, we observe only small Faradaic current change.

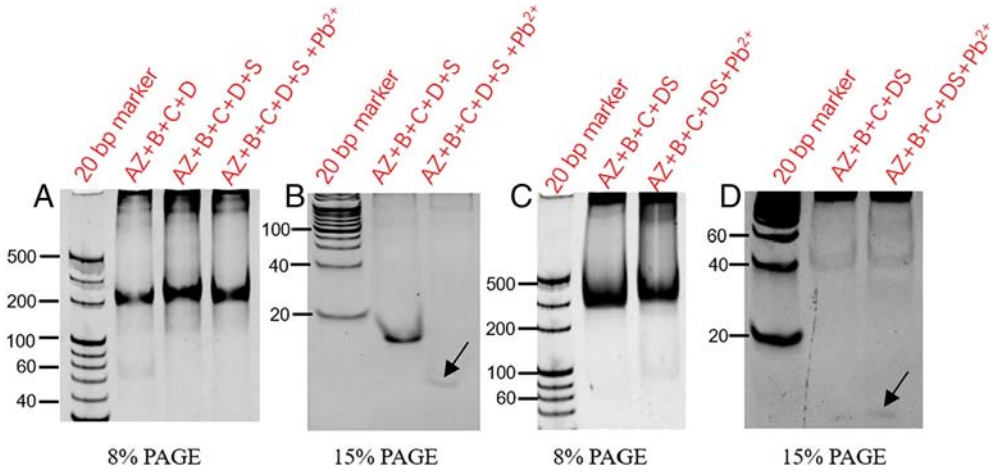

Figure 3. PAGE (8% and 15%) analysis of the enzymatic substrate-cleavage reaction with the tetrahedron. The concentration of all strands was 1 μM. **(A** and **B)** Electrophoretic results for the Model A enzymatic cleavage reaction with polyacrylamide concentrations of 8% and 15%, respectively. **(C** and **D)** Electrophoretic results of polyacrylamide gels of Model B and Model C at concentrations of 8% and 15%, respectively. The arrows in **B** and **C** indicate the new band products.

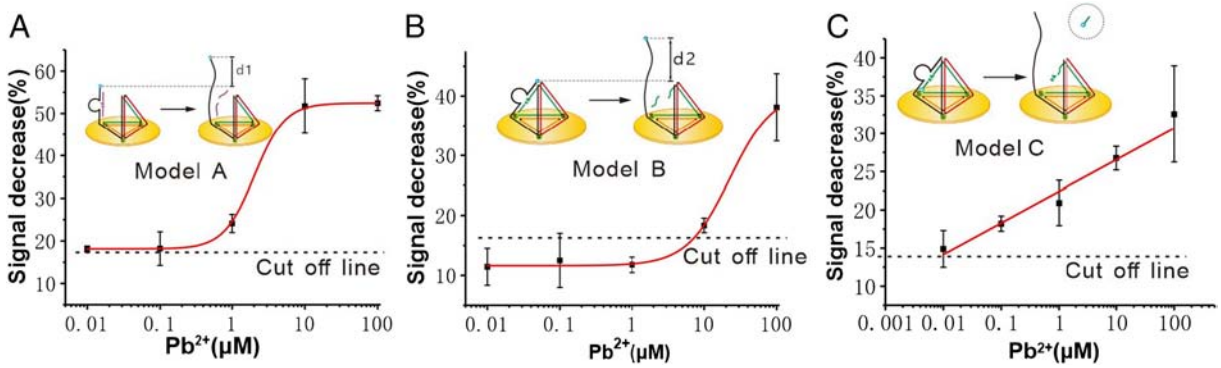

Figure 4. Simultaneous detection of various concentrations of Pb^{2+} (from 10.0 nM to 100.0 μM) with the three different types of DNAzyme tetrahedron nanoprobes. The figure is a schematic representation of the different structure designs. The error bars reflect the standard deviation of three independent measurements. The dashed line represents the percent decrease in the electrochemical signal of the control group.

Upon the increase of the Pb^{2+} concentration, we observed a large Faradaic current change. Model A is sensitive to detect as low as 0.1 μM Pb^{2+}. The percentage change of the measured current towards a target of 0.1 μM (18.41%) is still larger than the mean blank value (13.94%) plus 3 standard deviations (1.47%). These results confirmed that the nanoprobes could achieve sensitive detection of the target metal ions. As shown in Figure 4, *B*, the resulting change percentage of Faradaic currents exhibited semi-logarithmic linear relationships with the concentrations of the target metal ions in the range of 10-100 μM. Model B is sensitive to detect as low as 10 μM Pb^{2+}. The change percentage of the measured current from a target of 10 μM (18.39%) is still larger than the mean blank value (11.66%) plus 3 standard deviations (1.56%). As shown in Figure 4, *C*, the change percentage of Faradaic currents also presents semi-logarithm relationship along with the concentrations of the target Pb^{2+} from 0.01 μM to 100 μM. Model C is sensitive to detect as low as 0.01 μM Pb^{2+}. The percentage change of the measured current from a target of 0.01 μM (15.44%) is still larger than the mean blank value (11.79%) plus 3 standard deviations (1.00%). There is no significant difference in current change between the blank groups of the three models. The error bars shown here reflected the standard deviation of three independent measurements, and the cutoff line (dashed line in Figure 4) is the average current change percentage of the blank group plus 3 times the standard deviation of the current change. Table S2, Table S3 and Table S4 in the Supporting Information show the current signal change of the biosensor before and after the addition of Pb^{2+} for the three detection models. The CV and SWV curves for the three models are shown in Figure S2, Figure S3 and Figure S4 in Supporting Information.

Electrochemical signal analysis of tetrahedra with three different probe designs

The three models were found to have different detection limits and linear ranges of detection. Comparing Model A with Model B, we found that the detection limit of Model A (0.1 μM) was 100-fold lower than that of Model B (10 μM). Comparing Model B with Model C, we found that Model C had a lower

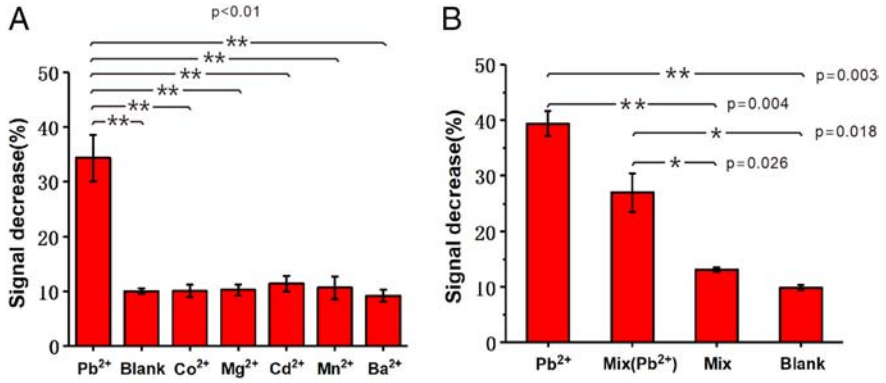

Figure 5. The Model C sensor was both specific (capable of rejecting similar ions) and selective (uninhibited by complex samples). **(A)** Little signal change was observed when the sensor was challenged with various divalent metal ions other than Pb^{2+} (all at 100 μM). The signal change for positive group is significantly different from that for the blank control ($P \ll 0.01$). **(B)** The sensor was selective enough to employ with mixed ions (all at 100 μM).

detection limit of 0.01 μM, which was 1000-fold better than Model B. The linear detection range of Model A was 1 μM to 10 μM, that for Model B was 10 μM to 100 μM, and that for Model C was 0.01 μM to 100 μM.

According to Xiao's work, we designed a DNA tetrahedron with one side consisting of a DNAzyme (Model A). Our initial analysis revealed that, in the presence of Pb^{2+}, a catalytic strand cleaves the edge of the DNA tetrahedron. These fragments presumably dissociate from the complex, allowing the electroactive group at the 5′ end of the A chain to collide freely with the electrode surface, in turn allowing the MB group to transfer electrons to the electrode and produce an increased signal (Figure 1, anticipation). However, our results showed a signal decrease, so we investigated the underlying cause of this unexpected result using Xiao's DNAzyme, a method of chemically detecting lead ions wherein a single strand of DNAzyme is assembled on the surface of a gold electrode. The substrate chain was later hybridized. After the cleavage reaction, the substrate chain is cut into two pieces, and the single strands with enzymatic properties are flexible to some extent. This flexibility causes the MB modified at the 5′ end of the DNAzyme chain to freely collide with the surface of the gold electrode, so that an increase in the current value can be detected. However, Model A involves a tetrahedron-based sensor, and the tetrahedron is constrained by steric hindrance on the surface of the gold electrode. Thus, the 5′ end of the AZM chain is not free to collide with the surface of the gold electrode, but stands upright in solution, which led to the decline of the Model A electrochemical signal. In addition, the Model A structure is not completely tetrahedral. The 5′ end of the A chain has a flexible structure. Thus, we designed Model B and Model C to further study the effect of the position of the electrochemically active group (MB) and the integrity of the tetrahedron on the performance of the detection platform. Our analysis was as follows.

The percentage of the signal decrease after the digestion of Pb^{2+} towards DNAzyme substrate should depend on the change of the effective distance between the MB and the electrode in Model A, B and C. For Model C, the MB is totally detached from the tetrahedral structure after digestion, and thus MB at this time has the largest distance from the electrode surface, so the detection performance is best. For Model A and Model B, the distance between MB and electrode surface is equal after digestion, so we need to compare the distance between the MB and the electrode surface before digestion. The difference is shown in the dotted circle in Figure 1. For model A, the DNAzyme can rotate around the bottom end, and tends to lie flat on the surface, making the effective distance of the methylene blue from the electrode shorter than Model B. The distance change between the electrochemically active group and the electrode in Model A is larger than that of Model B, so Model A exhibits higher detection performance.

Selectivity and specificity for detecting lead ions

Since Model C shows the best detection performance, it was chosen as an optimal detection model. As shown in Figure 5, the specificity of the sensor was determined by challenging it with the divalent metal ions, Co^{2+}, Mg^{2+}, Cd^{2+}, Mn^{2+}, and Ba^{2+} at a concentration of 100 μM. Figure 5, *A* shows that signal change of the positive group was significantly larger than the blank control and the five negative control groups containing different ions ($P \ll 0.01$). As shown in Figure 5, *B*, the signals from the two positive groups separately or mixed contained Pb^{2+} were distinguishable from the negative control groups when other metal ions were added. The sensor was demonstrated selective enough to employ with a mixed ion solution, which also suggests its stability from the interferences of other ions.

Detection of actual samples

Our biosensor (Model C) can detect Pb^{2+} in tap water and river water as shown in Figure 6. Electrochemical detection was performed by adding 0.1 or 10 μM lead ions. No significant signal change was observed with the blank group, although a clear signal change was found with the experimental group. In contrast, however, we found that the detection signal of tap water changed significantly more than that of river water. For example, the signal drop rate for the tap water-detection limit was significantly lower than that of tap water at a Pb^{2+}concentration of 10 μM. We speculate that the composition of river water is complex, containing microorganisms or RNases that could

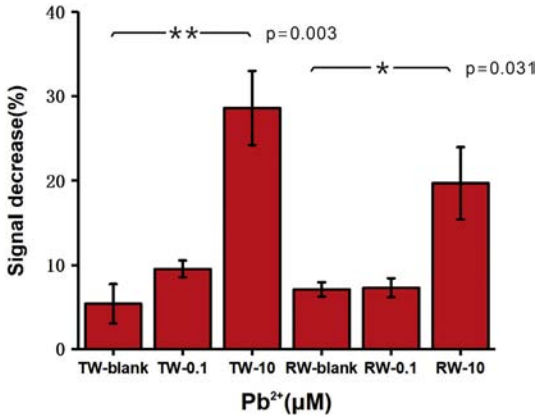

Figure 6. The detection of Pb^{2+} in tap water (TW) and river water (RW) samples with Model C. We added 0.1 or 10 μM lead ions for electrochemical detection, as indicated. No significant signal change was observed for the blank group. The positive group had a larger signal change. *P* values are displayed above the histogram.

cleave and inactivate the detection system. Therefore, among the blank groups samples, the river water showed more of a signal decrease than the tap water. The above test results suggest that the biosensor platform was also suitable for complex system samples from river and tap water, suggesting its stability.

Moreover, we also test its detection performance towards lead ions in soil extracts. As shown in Figure S5 in Supporting Information, the result presents statistically different between the blank group and the target group ($P = 0.003$). However, the signal difference for soil extracts is not so significant as that for tap or river samples. The interference might be from the possible negative effect of RNases present in soil extracts.

Conclusion

In summary, we designed a new biosensing interface to detect Pb^{2+} using a well-defined 3D DNA self-assembling nanostructure with one edge comprised of a DNAzyme. By comparing three models of DNA tetrahedron-based DNAzyme sensors, we found the impact of the tetrahedral DNA structure and the MB electrochemical active position on the signal response to Pb^{2+}. Along with the distance change between the electroactive group and the electrode surface, the limit of detection (LOD) concentration and the linear range of semi-logarithm could reach 0.01 μM and 0.01 μM-100 μM respectively. The sensitivity of our optimal detection method was improved by an order of magnitude (reaching 0.01 μM) versus the non-nanomaterial modified electrochemical method for Pb^{2+}. Model C not only showed good specificity for Pb^{2+} over other ions such Co^{2+}, Mg^{2+}, Cd^{2+}, Mn^{2+}, and Ba^{2+}, but also enabled Pb^{2+} detection with samples of tap water and river water. Our design strategy improved the performance of DNA tetrahedra for detecting Pb^{2+}, which could also enhance the understanding of how the tetrahedral structure and the position of electroactive groups affects electrochemical sensing of other analytes, based on the DNA tetrahedron-detection platform.

Appendix A. Supplementary data

Supplementary data to this article can be found online at https://doi.org/10.1016/j.nano.2019.102035.

References

1. Needleman H. Lead poisoning. *Annu Rev Med* 2004;**55**(1):209-22.
2. Needleman HL, Houk VN, Billick IH, Buchart E, Chadzynski L, Challop R, et al. Preventing lead poisoning in young children: a statement by the center for disease control. *J Pediatr* 1991;**93**(4):709-20.
3. Longerich HP, Fryer BJ, Strong DF. Determination of lead isotope ratios by inductively coupled plasma-mass spectrometry (ICP-MS). *Atomic Spectroscopy* 1987;**42**(1):39-48.
4. Bansod BK, Kumar T, Thakur R, Rana S, Singh I. A review on various electrochemical techniques for heavy metal ions detection with different sensing platforms. *Biosens Bioelectron* 2017;**94**:443-55.
5. Khoshbin Z, Housaindokht MR, Verdian A, Bozorgmehr MR. Simultaneous detection and determination of mercury (II) and lead (II) ions through the achievement of novel functional nucleic acid-based biosensors. *Biosens Bioelectron* 2018;**116**:130-47.
6. Kim HN, Ren WX, Kim JS, Yoon J. Fluorescent and colorimetric sensors for detection of lead, cadmium, and mercury ions. *Chem* 2012;**43**(29):3210-44.
7. Zhou G, Chang J, Cui S, Pu H, Wen Z, Chen J. Real-time, selective detection of Pb^{2+} in water using a reduced graphene oxide/gold nanoparticle field-effect transistor device. *ACS Appl Mater Interfaces* 2014;**6**(21):19235-41.
8. Chai F, Wang C, Wang T, Li L, Su Z. Colorimetric detection of Pb^{2+} using glutathione functionalized gold nanoparticles. *ACS Appl Mater Interfaces* 2010;**2**(5):1466-70.
9. Lotfi Zadeh Zhad HR, Lai RY. Application of calcium-binding motif of E-cadherin for electrochemical detection of Pb(II). *Anal Chem* 2018;**90**(11):6519-25.
10. Kokkinos C, Angelopoulou M, Economou A, Prodromidis M, Florou A, Haasnoot W, et al. Lab-on-a-membrane foldable devices for duplex drop-volume electrochemical biosensing using quantum dot tags. *Anal Chem* 2016;**88**(13):6897-904.
11. Liu J, Lu Y. A colorimetric lead biosensor using DNAzyme-directed assembly of gold nanoparticles. *J Am Chem Soc* 2003;**125**(22):6642-3.
12. Xiang Y, Lu Y. Using personal glucose meters and functional DNA sensors to quantify a variety of analytical targets. *Nat Chem* 2011;**3**(9):697-703.
13. Saran R, Yao L, Hoang P, Liu J. Folding of the silver aptamer in a DNAzyme probed by 2-aminopurine fluorescence. *Biochimie* 2018;**145**:145-50.
14. Liu H, Yu X, Chen Y, Zhang J, Wu B, Zheng L, et al. Crystal structure of an RNA-cleaving DNAzyme. *Nat Commun* 2017;**8**(1):1-10.
15. Laine M, Lönnberg T, Helkearo M, Lönnberg H. Cleavage of short oligoribonucleotides by a Zn^{2+} binding multi-nucleating azacrown conjugate. *Inorg Chim Acta* 2016;**452**:111-7.
16. Zhao XH, Kong RM, Zhang XB, Meng HM, Liu WN, Tan W, et al. Graphene-DNAzyme based biosensor for amplified fluorescence "turn-on" detection of Pb^{2+} with a high selectivity. *Anal Chem* 2011;**83**(13):5062-6.
17. Wang Y, Irudayaraj J. A SERS DNAzyme biosensor for lead ion detection. *Chem Commun* 2011;**47**(15):4394-6.
18. Li W, Yang Y, Chen J, Zhang Q, Wang Y, Wang F, et al. Detection of lead (II) ions with a DNAzyme and isothermal strand displacement signal amplification. *Biosens Bioelectron* 2014;**53**(1):245-9.
19. Liu M, Lou X, Du J, Guan M, Wang J, Ding X, et al. DNAzyme-based fluorescent microarray for highly selective and sensitive detection of lead (II). *Analyst* 2012;**137**(1):70-2.

20. Kim HK, Liu J, Li J, Nagraj N, Li M, Pavot MB, et al. Metal-dependent global folding and activity of the 8-17 DNAzyme studied by fluorescence resonance energy transfer. *J Am Chem Soc* 2007;**129**(21):6896-902.
21. Schlosser K, Li Y. A versatile endoribonuclease mimic made of DNA: characteristics and applications of the 8-17 RNA-cleaving DNAzyme. *Chembiochem* 2010;**11**(7):866-79.
22. Mazumdar D, Nagraj N, Kim HK, Meng X, Brown AK, Sun Q, et al. Activity, folding and Z-DNA formation of the 8-17 DNAzyme in the presence of monovalent ions. *J Am Chem Soc* 2009;**131**(15):5506-20.
23. Xiao Y, Rowe AA, Plaxco KW. Electrochemical detection of parts-per-billion lead via an electrode-bound DNAzyme assembly. *J Am Chem Soc* 2007;**129**(2):262-3.
24. Yun W, Cai D, Jiang J, Zhao P, Huang Y, Sang G. Enzyme-free and label-free ultra-sensitive colorimetric detection of Pb(2+) using molecular beacon and DNAzyme based amplification strategy. *Biosens Bioelectron* 2016;**80**:187-93.
25. Zhang Y, Li M, Li Z, Li Q, Aldalbahi A, Shi J, et al. Recognizing single phospholipid vesicle collisions on carbon fiber nanoelectrode. *Science China Chemistry* 2017;**60**(11):1474-80.
26. Su Y, Peng T, Xing F, Li D, Fan C. Nanoplasmonic biological sensing and imaging. *Acta Chim Sinica* 2017;**75**(11):1036-46.
27. Li J, Song S, Liu X, Wang L, Pan D, Huang Q, et al. Enzyme-based multi-component optical nanoprobes for sequence-specific detection of DNA hybridization. *Adv Mater* 2008;**20**(3):497-500.
28. Baldwin S, Deighan C, Bandeira E, Kwak KJ, Rahman M, Nana-Sinkam P, et al. Analyzing the miRNA content of extracellular vesicles by fluorescence nanoparticle tracking. *Nanomedicine: Nanotechnology Biology & Medicine* 2016;**13**(2):765-70.
29. Xun G, Tsou YH, Garis M, Huang H, Xu X. Highly specific colorimetric detection of DNA oxidation biomarker using gold nanoparticle/triplex DNA conjugates. *Nanomedicine: Nanotechnology Biology & Medicine* 2016;**12**(7):2101-5.
30. Yokchom R, Laiwejpithaya S, Maneeprakorn W, Tapaneeyakorn S, Rabablert J, Dharakul T. Paper-based immunosensor with signal amplification by enzyme-labeled anti-p16 INK4a multifunctionalized gold nanoparticles for cervical cancer screening. *Nanomedicine: Nanotechnology Biology & Medicine* 2018;**14**(3):1051-8.
31. Uddin MI, Jayagopal A, Wong A, Mccollum GW, Wright DW, Penn JS. Real-time imaging of VCAM-1 mRNA in TNF-α activated retinal microvascular endothelial cells using antisense hairpin-DNA functionalized gold nanoparticles. *Nanomedicine: Nanotechnology Biology & Medicine* 2017;**14**(1):63-71.
32. Goodman RP, Berry RM, Turberfield AJ. The single-step synthesis of a DNA tetrahedron. *Chem Commun* 2004;**12**(12):1372-3.
33. Peng G, Li X, Cui F, Qiu Q, Chen X, Huang H. Aflatoxin B1 electrochemical aptasensor based on tetrahedral DNA nanostructures functionalized three dimensionally ordered macroporous MoS2–AuNPs film. *ACS Appl Mater Interfaces* 2018;**10**(21):17551-9.
34. Miao P, Wang B, Chen X, Li X, Tang Y. Tetrahedral DNA nanostructure-based microRNA biosensor coupled with catalytic recycling of the analyte. *ACS Appl Mater Interfaces* 2015;**7**(11):6238-43.
35. Abi A, Lin M, Pei H, Fan C, Ferapontova EE, Zuo X. Electrochemical switching with 3D DNA tetrahedral nanostructures self-assembled at gold electrodes. *ACS Appl Mater Interfaces* 2014;**6**(11):8928-31.
36. Wen Y, Pei H, Wan Y, Su Y, Huang Q, Song S, et al. DNA nanostructure-decorated surfaces for enhanced aptamer-target binding and electrochemical cocaine sensors. *Anal Chem* 2011;**83**(19):7418-23.
37. Li N, Wang M, Gao X, Yu Z, Pan W, Wang H, et al. A DNA tetrahedron nanoprobe with controlled distance of dyes for multiple detection in living cells and in vivo. *Anal Chem* 2017;**89**(12):6670-7.
38. Wen Y, Pei H, Shen Y, Xi J, Lin M, Lu N, et al. DNA nanostructure-based interfacial engineering for PCR-free ultrasensitive electrochemical analysis of microRNA. *Sci Rep* 2012;**2**:867-73.
39. Bu NN, Tang CX, He XW, Yin XB. Tetrahedron-structured DNA and functional oligonucleotide for construction of an electrochemical DNA-based biosensor. *Chem Commun* 2011;**47**(27):7689-91.
40. Pei H, Lu N, Wen Y, Song S, Liu Y, Yan H, et al. A DNA nanostructure-based biomolecular probe carrier platform for electrochemical biosensing. *Adv Mater* 2010;**22**(42):4754-8.
41. Lin M, Wang J, Zhou G, Wang J, Wu N, Lu J, et al. Programmable engineering of a biosensing interface with tetrahedral DNA nanostructures for ultrasensitive DNA detection. *Angew Chem Int Ed* 2015;**54**(7):2151-5.
42. Dong SB, Zhao RT, Zhu JG, Lu X, Li Y, Qiu SF, et al. Electrochemical DNA biosensor based on a tetrahedral nanostructure probe for the detection of avian influenza a (H7N9) virus. *ACS Appl Mater Interfaces* 2015;**7**(16):8834-42.
43. Pinheiro AV, Nangreave J, Jiang S, Yan H, Liu Y. Steric crowding and the kinetics of DNA hybridization within a DNA nanostructure system. *ACS Nano* 2012;**6**(6):5521-30.
44. Shen J, Li Y, Gu H, Xia F, Zuo X. Recent development of sandwich assay based on the nanobiotechnologies for proteins, nucleic acids, small molecules, and ions. *Chem Rev* 2014;**114**(15):7631-77.
45. Song P, Li M, Shen J, Pei H, Chao J, Su S, et al. Dynamic modulation of DNA dybridization using allosteric DNA tetrahedral nanostructures. *Anal Chem* 2016;**88**(16):8043-9.
46. Zhu D, Pei H, Yao G, Wang L, Su S, Chao J, et al. A surface-confined proton-driven DNA pump using a dynamic 3D DNA scaffold. *Adv Mater* 2016;**28**(32):6860-5.
47. Ge Z, Lin M, Wang P, Pei H, Yan J, Shi J, et al. Hybridization chain reaction amplification of microRNA detection with a tetrahedral DNA nanostructure-based electrochemical biosensor. *Anal Chem* 2014;**86**(4):2124-30.
48. Lin M, Song P, Zhou G, Zuo X, Aldalbahi A, Lou X, et al. Electrochemical detection of nucleic acids, proteins, small molecules and cells using a DNA-nanostructure-based universal biosensing platform. *Nat Protoc* 2016;**11**(7):1244-63.
49. Zhou W, Liang W, Li D, Yuan R, Xiang Y. Dual-color encoded DNAzyme nanostructures for multiplexed detection of intracellular metal ions in living cells. *Biosens Bioelectron* 2016;**85**:573-9.